A Robust Response of the Hadley Circulation to Global Warming

William K. M. Lau and K. M. Kim

Earth Science Division,

NASA/Goddard Space Flight Center

Greenbelt, MD 20771

January, 2014

Submitted to Nature Geoscience

Abstract

Tropical rainfall is expected to increase in a warmer climate. Yet, recent studies have inferred that the Hadley Circulation (HC), which is primarily driven by latent heating from tropical rainfall, is weakened under global warming. Here, we show evidence of a robust intensification of the HC from analyses of 33 CMIP5 model projections under a scenario of 1% per year CO_2 emission increase. The intensification is manifested in a "deep-tropics squeeze", characterized by a pronounced increase in the zonal mean ascending motion in the mid and upper troposphere, a deepening and narrowing of the convective zone and enhanced rainfall in the deep tropics. These changes occur in conjunction with a rise in the region of maximum outflow of the HC, with accelerated meridional mass outflow in the uppermost branch of the HC away from the equator, coupled to a weakened inflow in the return branches of the HC in the lower troposphere.

1. Introduction

The Hadley Circulation (HC), the zonally averaged meridional overturning cell connecting the tropics and mid-latitude, is a key component of the global atmospheric general circulation. How the HC has been, or will be changed as a result of global warming has tremendous societal implications on changes in weather and climate patterns, especially the occurrences of severe floods and droughts around the world [1-3]. Recent studies have argued that because of the balance requirement for water vapor and precipitation, the tropical circulation has to be weakened as a result of global warming [4-6]. Numerous authors have cited the weakening of the Walker Circulation in global warming experiments as an evidence of weakening of the tropical circulation [5,6]. Others have emphasized that the weakening of the Walker circulation is due to global warming induced equatorial sea surface temperature east-west gradient, rather than a result of the water vapor-precipitation constraint [7,8]. Analysis of observations of long-term (~30 years) tropical rainfall showed that the Walker Circulation actually has been strengthening in recent decades, suggesting that the tropical circulation may have been more strongly affected by natural variability [9-11]. While it is generally agreed that the rate of global precipitation change and water recycling time are strongly controlled by atmospheric radiation balance especially longwave radiative cooling, regional rainfall anomalies are more likely to be controlled by local changes in circulation and surface energy fluxes [12-14]. Even though a robust signal in the widening of the subtropics associated with the expansion of the HC under global warming has been found in climate model projections and observations [6, 15-19], a weakening of HC has yet to be demonstrated convincingly. Observations based on reanalysis data have shown weak signals of increasing, decreasing or no change in HC strength in recent decades [20-22] depending on the data source and the period of analyses. Particularly, reanalysis wind and moisture data in the

tropical upper atmosphere are subject to large biases, and extreme caution has to be exercised in the use of these data for trend detection for the HC [21, 23].

Previous theoretical studies have found that the HC is very sensitive to heating in the deep tropics, *i.e.*, a small increase in heating concentrated near the equator can lead to significant strengthening of the HC [24,25]. One of the major difficulties with the notion of a weakening of the tropical circulation is that rainfall in the deep tropics have been shown to be increasing due to global warming in model simulations [3, 7, 26-28], and in multi-decadal satellite rainfall observations [29,30]. Increased rainfall in the deep tropics will be associated with enhanced condensational heating, and therefore overall strengthening of tropical circulation as represented by the HC. Hence the paradigm of weakening tropical circulation associated with global warming is confronted with some perplexing questions. How can a weakened tropical circulation be compatible with increased tropical rainfall? Why is there no obvious signal of weakening or strengthening of the HC in observations and in GCM simulations, given that it is the most basic representation of the tropical circulation? In this paper, we show evidence of an intensification of the HC under global warming, as manifested in enhanced ascent in the rising branch of the HC, a deepening of tropical convection, a narrowing of the convective zone in the deep tropics, and enhanced rainfall in the equatorial central and eastern Pacific.

2. Results

To establish the baseline response of the HC to greenhouse gas (GHG) warming, we used outputs from a 140-year integration of each of 33 CMIP5 (Coupled Model Intercomparison Project -5) models forced by 1% increase per year CO_2 emission to explore the response of the HC to global warming (See Data and Method in Supplementary Material for details). Effects

from other greenhouse gases besides CO_2 and aerosols are not considered here. The control, also referred to as climatology, is defined as the first 25 years of the 140-year model simulation. By the mid-point of the integration, *i.e.*, 25-years centered at year-70 of the integration, the CO_2 level is nearly doubled (DCO2), and by the last 25-year, the CO_2 level is nearly tripled (TCO2). In this work, we only focused on the forced response, as represented by the Multi Model Mean (MMM), defined as the average of all 33 models. The uncertainties of the MMM are estimated from the standard deviation between individual models and the MMM. Anomalies are defined as the MMM difference between either DCO2, or TCO2 with respect to the control. Because the conclusions are essentially the same for DCO2 and TCO2 except for higher signal-to-noise ratio in the latter, results shown in this paper are for TCO2, unless otherwise stated.

Vertical motions

Consistent with previous studies [3-6], we find that in response to a 1% per year CO_2 increase , the MMM global temperature and rainfall increases steadily, with an estimated rainfall sensitivity of $1.5 \pm 0.1\%\ K^{-1}$ much slower than that for saturated water vapor as governed by the Clausius-Clapeyron relationship ($\sim 7\%\ K^{-1}$). The associated changes in the large-scale tropical circulation as reflected in the mid-tropospheric (500hPa) vertical motions averaged over different latitudinal width are shown in Fig. 1. In the near-equatorial regions (5^oS-5^oN), there is a robust increasing trend in upward motion as indicated by the near constant positive slope ($\sim 5.2\pm1.0\ \%\ K^{-1}$) and the small spread among the models. At wider latitude bands (10^oS-10^oN and 20^oS-20^oN), the changes in vertical motions are substantially muted. When the zonal averages are taken over the entire tropics (30^oS-30^oN), the vertical motions again show a robust rise, but with much smaller amplitude compared to 5^oS-5^oN. Based on the similar signs of the control and the trends, these results indicate that global warming induces enhanced mean rising motion

89 over the entire tropics (30°S-30°N), with the most contributions coming from the near equatorial
90 region (5°S-5°N).

91 To better understand the response, we examine the relationship between zonally averaged
92 rainfall and vertical motions (Fig. 2). Both the climatological MMM rainfall and 500 hPa
93 pressure velocity show double maxima in the tropics, with a minimum over the equator,
94 consistent with the observed off- equatorial positions of the Inter-Tropical Convergence Zones
95 (ITCZ) [31]. The anomalous rainfall profile shows pronounced increase in rainfall between 10°S
96 and 10°N, a widening of the subtropical dry zones, and increase rainfall in the extratropics of
97 both hemispheres (Fig. 2a). The anomalous pressure velocity profile (Fig.2b) features wavelike
98 perturbations that generally have signs opposite to the climatology, with enhanced anomalous
99 rising motion coinciding with increased rainfall in the deep tropics. Strong compensating
100 anomalous sinking motions are found centered near 10°S and 10°N, which appear to be coupled
101 with anomalous rising motion in the subtropics centered around 25-30° N and S.
102 Comparing the vertical profiles of the pressure velocity in the control (Fig. 2c) with the anomaly
103 (Fig.2d), a structural change can be perceived in the form of a narrowing and stronger anomalous
104 ascent throughout the troposphere in the equatorial region, flanked on both sides by equally
105 strong descent centered near 10°S and 10°N. This creates the appearance of a filling-in of the
106 climatological equatorial minimum by a "squeeze" of the ascending branch of the HC toward the
107 equator from both hemispheres. This "deep–tropics squeeze" (DTS) appears to be coupled to
108 positive anomalies, *i.e.,* weakened sinking motions, near the center of the climatological
109 subsiding branches of the HC. A widening of the subtropics is achieved via the DTS together
110 with a poleward extension (marked by zero-wind contours) of the sinking branch of the HC.
111 Associated with structural changes in the vertical motions of the HC are also poleward shifts of

112 the Ferrel and polar cells in both hemispheres, as indicated by the positions of the anomalous
113 positive and negative centers, and the zero-vertical motion lines. These changes in the HC and
114 related global signals are robust in the sense that more than two-third (25/33) of the models agree
115 on the sign of the anomalies (grid points highlighted by a green dot in Fig. 2d) almost
116 everywhere.

117 *Tropical Convection*

118 To understand the nature of the DTS, we examine the changes in tropical convection and the
119 large-scale tropical circulation. Here, as a proxy for tropical convection, monthly outgoing
120 longwave radiation, OLR will be used. Based on a comparison of observations between monthly
121 OLR from NOAA AVHRR, and daily brightness temperature from TRMM (For details see Fig.
122 S1 and discussions in Supplementary Material), a high OLR (>270Wm^{-2}) can be identified
123 crudely with the predominance of low level liquid-phase clouds; a moderate OLR (270 -220
124 Wm^{-2}) with mid-level mixed phase clouds, and a low OLR (<220Wm^{-2}) with deep, ice-phase
125 clouds and deep convection [32-35]. We have computed the MMM climatological probability
126 distribution functions (pdf) of OLR and their changes due to global warming. The climatological
127 OLR pdf (Fig. 3a, b) indicates a weak bimodal distribution of convection in the deep tropics,
128 with an abundance of low to mid-level liquid clouds and mixed phase clouds, as well as ice-
129 phase clouds (OLR < 220 Wm^{-2}) associated with deep tropical convection. Near the equator
130 (Fig. 3a), the anomalous OLR profile indicates a shift toward deeper convection, as evident in
131 the pronounced increase in the frequency of lower OLR (colder cloud top) and decrease in higher
132 OLR (warmer cloud top) in the range of 5-15% At 10^{o}S-10^{o}N, similar shift toward deeper
133 convection can be seen, though the signal is weaker (< 10%) compared to near the equator, due
134 to the anomalous subsidence near 10^{o}S and N. (See also Fig. 2). As more of the subtropics is

included (See Fig. S2 in Supplementary Material), the deeper convection signal is weakened substantially, while a slight increase in the very low and warm (OLR~300 Wm^{-2}) clouds begins to emerge [33,34]. The deepening of convection is consistent with the increase in upward velocity in the ascending branch of the HC (Fig. 3c and d). The anomalous vertical motion is characterized by an overall enhanced ascent at all levels, most pronounced (up to ~30-40% increase) at upper levels, signaling an upward shift of maximum ascent from the lower to mid-troposphere (700-300 hPa) to the upper troposphere (300-150 hPa). Averaged over 10^oS -10^oN, the enhanced ascent in the upper troposphere is still strong (~ 30%), but the anomalous vertical motion below 300 hPa is slightly negative, implying a weakened climatological ascending motion (Fig. 3b) in the lower troposphere. The overall slight weakening in the lower troposphere is due to strong anomalous sinking motions found near 10^oS and 10^oN, associated with the DTS.

Meridional outflow and jetstreams

The DTS is closely tied to changes in the HC meridional outflow (Fig. 4). Here, the most prominent feature is a vertical dipole wind anomaly, with opposite signs in each hemisphere, *i.e.*, a quadruple pattern, with enhanced outflow away from the equator in the 200 -100 hPa layer, and increased inflow between 400-200hPa, toward the equator. Comparing to the control, this signals a rise in the region of maximum outflow in the upper branch of the HC from its climatological maximum height near 200 hPa to 150 hPa. An examination of the anomalous meridional wind profiles for each model (Supplementary Material Fig. S3) indicates that the rise of the maximum outflow region of the HC under global warming is very robust, with all 33 models showing the characteristic quadruple pattern, albeit with varying magnitudes. The rise in the region of maximum outflow of the HC is consistent with the increase in tropopause height in the tropics under global warming reported in past studies [36-38].

158 Changes in the HC associated with the DTS and their connection to the global circulations
159 can be clearly seen in the anomalous meridional mass streamfunction and zonal winds (Fig. 5).
160 From the signs and locations of the anomalies compared to the control (Fig. 5a), it is clear that
161 the upper branches (above 250 hPa) of the HC in the deep tropics is strengthened, while the
162 lower portion (1000-300 hPa) is weakened, consistent with an elevation of the climatological
163 region of maximum outflow, *i.e.*, a rise of the center of mass, of the HC. The rise together with
164 deeper convection in the ascending branch of the HC allow stronger poleward outflow in the
165 upper troposphere (see also Fig. 4), thus extending the subsidence branches of the HC in both
166 hemispheres further poleward from their climatological positions. A similar polar extension of
167 the Ferrel cells in both hemispheres, though with much smaller amplitude, can also be discerned.
168 The rise of the center of maximum outflow in the upper branch of the HC is also reflected in
169 changes in the structure of the zonal wind anomaly (Fig. 5b). The most pronounced zonal wind
170 acceleration is found near 100 hPa, above the climatological center at 150- 200 hPa in both
171 hemispheres. The subtropical westerly acceleration in both hemispheres is likely to be driven
172 by the deeper convection, and the coriolis force from the stronger outflow in the upper
173 troposphere associated with the meridional wind dipole anomalies noted previously. The
174 extratropical maximum may be related to the enhanced baroclinicity due to increased
175 temperature gradient at the upper troposphere, and polar shift of the wintertime storm tracks [39,40].
176 As shown in Supplementary Material (Fig. S4 and S5), the meridional streamfunction and zonal
177 winds exhibit pronounced seasonality with the strongest deepening of the HC and upper
178 troposphere outflow from the summer to the winter hemisphere, with maximum response in the
179 wintertime jetstreams.

The time evolution of the meridional wind dipole anomaly at 10^{o} N and S respectively (Fig. 6) shows an increasingly stronger (weaker) outflow above (below) 200 hPa, in both hemispheres, as the CO_2 concentration increases. The near constant positive slopes of the total wind isotachs above 200 hPa reflect a steady rise (~3.5 hPa decade^{-1}) of the region of maximum outflow of the HC. Computations of the meridional mass flux, *i.e.*, mass weighted meridional wind at different cross-sections (See details in discussion of Table S1 in Supplementary Material) show that the mass outflow at the upper portion (200-100hPa) out of the 10^{o}S-10^{o}N zone is intensifying at a fast rate of +9.8±0.7 % K^{-1}. The rate of increase is even faster at +17.0±1.7%K^{-1}, out of the 5^{o}S-5^{o}N zone which corresponds to the core ascending branch of the HC. The increased meridional mass flux is compensated by strong inflow in the lower portion (400-200 hPa) of the climatological outflow region. Even with the strong compensation, the net anomalous mass flux over the climatological outflow region (400-100hPa) out of the 5^{o}S-5^{o}N zone is still increasing, albeit at a much reduced net rate of 1.9±0.8% K^{-1}. At 10^{o}S-10^{o}N, the net mass flux in the climatological outflow zone shows a weak decline at 1.2±0.3% K^{-1}, due to the negative mass flux in the lower portion of the outflow region. The weakening may be related to the increased vertical static stability associated with the deepening of tropical convection, and the stronger warming of the upper relative to the lower tropical troposphere under global warming [41]. In contrast to the upper troposphere, changes in the zonal mean meridional wind below 400 hPa are relatively muted, and contribute little to the wind response of the HC. However, because the abundance of water vapor in the lower troposphere, even relatively small changes in meridional winds could induce large changes in moisture transport and convergence, contributing significantly to regional precipitation anomalies including the formation of new dry zones in the

marginal convective regions over tropical land through atmosphere-land feedback processes[3, 26, 42].

3. Comparison with previous studies

Our findings regarding the DTS and associated deepening and intensifying of the upper branch of the HC induced by increased CO_2 is significantly different from prevailing view of the weakening of the tropical circulation under global warming. We believe that previous studies [5,6] conflated a global circulation slow down constrained by global water cycle balance requirement, with a tropical circulation change based on the response of the Walker circulation due to changes in tropical east-west sea surface temperature gradient. The HC, which represents the totality of all tropical motions, should be the true measure of tropical circulation change. Many studies [4-6] used measures of tropical circulation defined by changes in vertical velocity over climatological ascent regions only, ignoring the large increase in latent heating due to increase in heavy precipitation over the central and equatorial Pacific, and the Arabian Sea which are located in climatological descent regions (Supplementary Fig. S6). These precipitation anomalies are likely driven by global warming induced sea surface temperature anomalies [7]. Focusing only on the climatological ascending regions resulted in an apparent weakening of the climatological vertical motion at all tropical latitudes, even in the deep tropics (Supplementary Fig. S7). However, this apparent weakening of the tropical circulation is associated with the change in the rising branch of the Walker circulation only. It does not take into account the net anomalous heating within the deep tropics, which is contributed strongly from the atmosphere over the equatorial central and eastern Pacific [3, 26, 35] (Fig. S6). Previous studies [21,22] using traditional single metric to define the HC, such as the maximum value at the climatological center of the

meridional mass streamfunction, or at the center of velocity potential at 200hPa also missed the non-uniform nature of the HC response reported here.

4. Concluding remarks

Based on analyses of outputs of 33 CMIP5 coupled models, we find that a robust intensification of the HC in response to a prescribed 1% increase per year in CO_2 emission. The intensification is associated with a deep-tropics-squeeze (DTS) anomaly pattern, manifested in enhanced ascent in the rising branch of the HC, a deepening and narrowing of the convective zone in the near equatorial regions, and a substantial increase in meridional mass outflow in the uppermost branch (200-100 hPa). The increase is associated with an upward shift of the region of maximum outflow of the HC, coupled to a widening of the subtropics, slower return inflow of the HC in the lower troposphere, as well as poleward migrations of the Ferrel and polar cells in both hemispheres. These changes in the large-scale circulation are consistent with changes in global precipitation pattern, satisfying the constraint of global precipitation-water vapor balance, while dynamically consistent with increased rainfall and latent heat of condensation in the deep tropics under global warming.

241 **Reference**

242 1. Diaz, H. F. & Bradley, R. S., Ed, *The Hadley Circulation: Present, Past and Future*
243 (Kluwer Academic Publisher, 2004).
244 2. Dai, A., Drought under global warming: a review. *WIREs Clim Change 2*, 45–65.
245 doi: 10.1002/wcc.81 (2011).
246 3. Lau, K. M., Wu, H. T. & Kim, K.M. A canonical response in rainfall characteristics to
247 global warming from CMIP5 model projections. *Geophys. Res. Lett*. **40**,
248 doi:10.1002/grl.50420 (2013).
249 4. Held, I. M. & Soden, B. J., Robust responses of the hydrological cycle to global
250 warming. *J. Climate* **19**, 5686–5699 (2006).
251 5. Vecchi, G. A. *et al*., Weakening of tropical Pacific atmospheric circulation due to
252 anthropogenic forcing, *Nature* **441**, 73–76, doi:10.1038/nature04744 (2006).
253 6. Vecchi, G. A. & Soden, B. J., Global warming and the weakening of the tropical
254 circulation. *J. Climate* **20**, 4316– 4340 (2007).
255 7. Xie, S.-P., *et al*., Global Warming Pattern Formation: Sea Surface Temperature and
256 Rainfall. *J. Climate*, **23**, 966–986. doi: http://dx.doi.org/10.1175/2009JCLI3329.1 (2010).
257 8. Tokinaga, H., Xie, S.-P., Deser, C., Kosaka, Y. & Okumura, Y. M., Slowdown of the
258 Walker circulation driven by tropical Indo-Pacific warming. *Nature*, **491**,
259 doi:10.1038/nature11576 (2012).
260 *9.* Sohn, B. J. &Park, S.-C.*,* Strengthened tropical circulations in past three decades
261 inferred from water vapor transport*. J. Geophys. Res*. **115***,* D15112,
262 doi:10.1029/2009JD013713 (2010).

10. L'Heureux, M. L., Lee, S. & Lyon, B., Recent multidecadal strengthening of the Walker circulation across the tropical Pacific. *Nature Climate Change* **3**, 571-576, doi:10.1038/NCLIMATE1840 (2013).
11. Kang, S. M., Deser, C. & Polvani, L. M., Uncertainty in Climate Change Projections of the Hadley Circulation: The Role of Internal Variability. *J. Climate* **26**, 7541–7554. doi: http://dx.doi.org/10.1175/JCLI-D-12-00788.1 (2013).
12. Stephens, G L & Ellis, T. D., Controls of global-mean precipitation increases in global warming GCM experiments. *J. Climate* **21** 6141–55 (2008)
13. Stephens, G. L. & Hu, Y., Are climate-related changes to the character of global precipitation predictable? *Environ. Res. Lett.* **5**, doi:10.1088/1748-9326/5/2/025209 (2010).
14. Hartmann, D., Tropical Surprise, *Science* **295**, 811, doi:10.1126/Science.1068447 (2002).
15. Frierson, D. M. W., Lu, J. & Chen, G., The width of the Hadley cell in simple and comprehensive general circulation models. *Geophys. Res. Lett*. **34**, L18804, doi:10.1029/2007GL031115 (2007).
16. Hu, Y. & Fu, Q., Observed poleward expansion of the Hadley circulation since 1979. *Atmos. Chem. Phys*. **7**, 5229–5236 (2007).
17. Lu, J., Vecchi, G. A. & T. Reichler, Expansion of the Hadley cell under global warming. *Geophys. Res. Lett*. **34**, L06805, doi:10.1029/2006GL028443 (2007).
18. Seidel, D. J. & Randel, R. J., Recent widening of the tropical belt: Evidence from tropopause observations. *J. Geophys. Res*. **112**, D20113, doi:10.1029/2007JD008861 (2007).

19. Seidel, D. J., Fu, Q., Randel, W. J. & Reichler, T. J., Widening of the tropical belt in a changing climate. *Nat. Geosci*. **1**, 21–24 (2008).

20. Quan, X.-W., Diaz, H. F. & Hoerling, M. P., in *The Hadley Circulation: Past, Present, and Future*, H. F. Diaz, R. S. Bradley, Eds.,(Springer, 2004), pp. 85–120.

21. Mitas, C. M. & Clement, A., Has the Hadley cell been strengthening in recent decades? *Geophys. Res. Lett*. **32**, L03809, doi:10.1029/2004GL021765 (2005).

22. Tanaka, H. L., Ishizaki, N. & Nohara, D., Intercomparison of the intensities and trends of Hadley, Walker and monsoon circulations in the global warming projections. *SOLA*, **1**, 77–80 (2005).

23. Waliser, D. E., Shi, Z., Lanzante, J. R., & Oort, A. H., The Hadley circulation: assessing NCEP/NCAR reanalysis and sparse in-situ estimates. *Clim. Dyn*. **15**, 719–735, doi:10.1007/s003820050312 (1999).

24. Hou, A. & Lindzen, R., The influence of concentrated heating on the Hadley circulation. *J. Atmos. Sci*. **49**, 1233-1241 (1992)

25. Waliser, D. E. & Somerville, R. C. J., Preferred Latitudes of the Intertropical Convergence Zone. *J. Atmos. Sci.* **51**, 1619–1639 (1994).

26. Meehl, G., Mu¨nnich, M., Su, H., Meyerson, J. E. & Holloway, C. E., Tropical drying trends in global warming models and observations. *Proc. Natl. Acad. Sci. USA* **103**, 6110–6115 (2006).

27. Meehl, G. A., *et al.,* in *Climate Change 2007: The Physical Science Basis*, S. Solomon et al., Eds., Cambridge University Press , pp. 747–845 (2007).

307 28. Chou, C., Neelin, J. D., Chen, C. A. & Tu, J.-Y., Evaluating the ‘‘rich-get-richer’’
308 mechanism in tropical precipitation change under global warming. *J. Climate* **22**, 1982–
309 2005 (2009)..
310 29. Lau, K. M. & Wu, H.-T., Trends in tropical rainfall characteristic, 1979-2003. *Int.. J.*
311 *Climatology* **27**, 979-988, doi:10.1002/joc.1454 (2007).
312 30. Zhou, Y. P., Xu, K.-M., Sud, Y. C. & Betts, A. K., Recent trends of the tropical
313 hydrological cycle inferred from Global Precipitation Climatology Project and
314 International Satellite Cloud Climatology Project data. *J. Geophys. Res*. **116**, D09101,
315 doi:10.1029/ 2010JD015197 (2011).
316 31. Adler, R. F., Huffman, G. J., Bolvin, D. T., Curtis, S. & Nelkin, E. J., Tropical rainfall
317 distributions determined using TRMM combined with other satellite and rain gauge
318 information. *J. Appl. Meteor.*, **39**, 2007–2023 (2000).
319 32. Masunaga, H. & Kummerow, C. D., Observations of tropical precipitating clouds
320 ranging from shallow to deep convective systems. *Geophy. Res. Lett*. **33**, L16805, doi:
321 10.1029/2006GL026547 (2006).
322 33. Lau, K.-M. & Wu, H. T., Climatology and changes in tropical oceanic rainfall
323 characteristics inferred from Tropical Rainfall Measuring Mission (TRMM) data (1998–
324 2009). *J. Geophys. Res*. **116**, D17111, doi:10.1029/2011JD015827 (2011).
325 34. Lau K.-M. & Wu, H. T., Warm Rain Processes Over Tropical Oceans and Climate
326 Implications. *Geophys. Res. Lett.* **30**, 2290, doi:10.1029/2003GL018567 (2003).
327 35. Chou, C. & Neelin, J. D., Mechanisms of global warming impacts on regional tropical
328 precipitation, *J. Climate*. **17**, 2688–2701 (2004).

36. Lorenz, D. J. & DeWeaver, E. T., Tropopause height and zonal wind response to global warming in the IPCC scenario integrations. *J. Geophys. Res*., **112**, D10119, doi:10.1029/2006JD008087 (2007).

37. Wilcox, L. J., Hoskins, B. J. & Shine, K. P., A global blended tropopause based on ERA data. Part II: Trends and tropical broadening. *Q. J. R. Meteorol. Soc*. **138**, 576-584. Doi:10.1002/qj.910 (2012).

38. O'Gorman, P. A. & Singh, M. S., Vertical structure of warming consistent with an upward shift in the middle and upper tropospher. *Geophys. Res. Lett*. **40**, 1838-1842, doi:10.1002/grl.50328 (2013).

39. Lu, J., Chen, G. & Frierson, D. M. W., Response of the Zonal Mean Atmospheric Circulation to El Niño versus Global Warming. *J. Climate* **21**, 5835–5851. doi: http://dx.doi.org/10.1175/2008JCLI2200.1 (2008).

40. Kushner, P. J., Held, I. M. & Delworth, T. L., Southern Hemisphere Atmospheric Circulation Response to Global Warming. *J. Climate* **14**, 2238–2249 (2001).

41. Chou, C. & Chen, A., Depth of tropical convection and weakening of the tropical circulation under global warming. *J. Climate* **25**, 3019-3030, DOI: 10.1175/2010JCLI3383.1 (2010).

42. Lintner, B. R., *et al*., Amplification of wet and dry month occurrence over tropical land regions in response to global warming. *J. Geophys.Res*. **117**, D11106, doi:10.1029/2012JD017499 (2012).

352

353 **Author contributions**

354 WKL & KMK conceived the motivation and analysis methodology of this work. KMK was responsible
355 for processing of the CMIP5 outputs and data analysis. WKL led the writing of this manuscript.

356 **Competing financial interests**

357 The authors declare no competing finacial interests.

358

359 **Figure Captions**

360 Figure 1 Time series of 140 simulated years of MMM 500 hPa vertical motion averaged
361 between a) 5^{o}S-5^{o}N, b)10^{o}S-10^{o}N, c) 20^{o}S-20^{o}N, d) 30^{o}S-30^{o}N, under 1% per year increase
362 CO_2 emission scenario. The MMM is computed from 33 CMIP5 models and the model
363 spread (yellow shading) is the standard errors of the MMM. Unit is negative Pa s^{-1}. The
364 number in the lower right hand corner indicates the MMM vertical velocity in the control.

365 Figure 2 Latitudinal profile of MMM (a) rainfall, and (b) 500 hPa vertical motion .
366 Climatology is indicated by red line and anomaly by black line. Open circles indicate
367 where more than 75% (25/33) models agree in the sign of the anomalies. Latitude-height
368 profile of MMM 500 hPa vertical motion for (c) climatology and (d) anomaly. Grid points
369 where more than 25 models agree in the sign of the anomaly are indicated by green dots.
370 Rainfall is in unit of mm day^{-1}, and vertical motion is in unit of negative Pa s^{-1}. Different
371 unit scales are used for climatology and anomalies.

Figure 3 Vertical profiles of MMM outgoing longwave radiation (OLR) probability distribution function averaged over (a) 5^oS-5^oN, and (b) 10^oS-10^oN. Vertical profile of mean vertical motion averaged over (c) 5^oS-5^oN, and (d) 10^oS-10^oN. Climatology is indicated by green line and anomaly by dotted line. The model spread is shown as yellow shading. The magnitudes of the anomalies have been doubled to enhance clarity. Vertical motion is in unit of negative Pa s^{-1}. Unit of OLR is Wm^{-2}.

Figure 4 Latitude-height cross-section of MMM meridional winds in the tropics. Climatology is shown in contours, anomaly in color. Unit is in ms^{-1}.

Figure 5 Latitude-height cross-section of MMM for a) merdional mass streamfunction (10^{10} Kg s^{-1}) , and b) zonal mean wind (ms^{-1}). MMM climatology is shown in contour, and anomaly in color. For meridional streamfunction, positive (negative) contours indicate clockwise (anticlockwise) circulation around the center of action.

Figure 6 Time-height cross-section of MMM zonally averaged meridional winds (ms^{-1}) for 140 simulated years, under 1% per year CO_2 increase, across a) 10^oN and b) 10^oS. Contours denote the total winds, solid (dotted) lines for positive (negative) winds. Wind anomalies are denoted by color shading. In the northern hemisphere (southern hemisphere), outflow away from the equator is denoted by positive (negative) values, and opposite for inflow toward the equator.

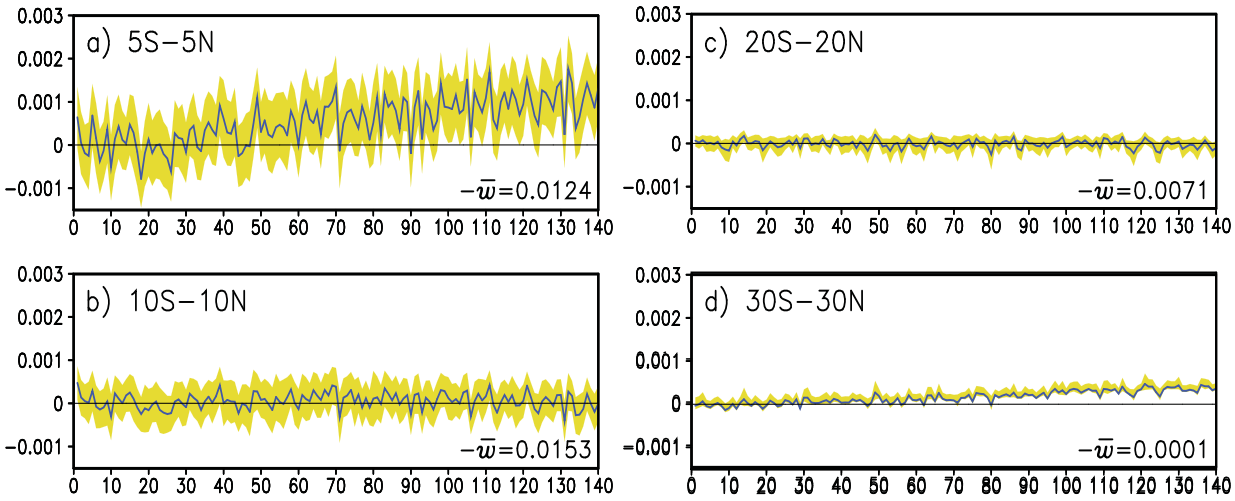

391

392 Figure 1 Time series of 140 simulated years of MMM 500 hPa vertical motion averaged between a) 5°S-
393 5°N, b)10°S-10°N, c) 20°S-20°N, d) 30°S-30°N, under 1% per year increase CO_2 emission scenario.
394 The MMM is computed from 33 CMIP5 models and the model spread (yellow shading) is the
395 standard errors of the mean of the 33 models. Unit is negative Pa s^{-1}. The number in the lower
396 right hand corner indicates the MMM vertical velocity in the control.

397

398

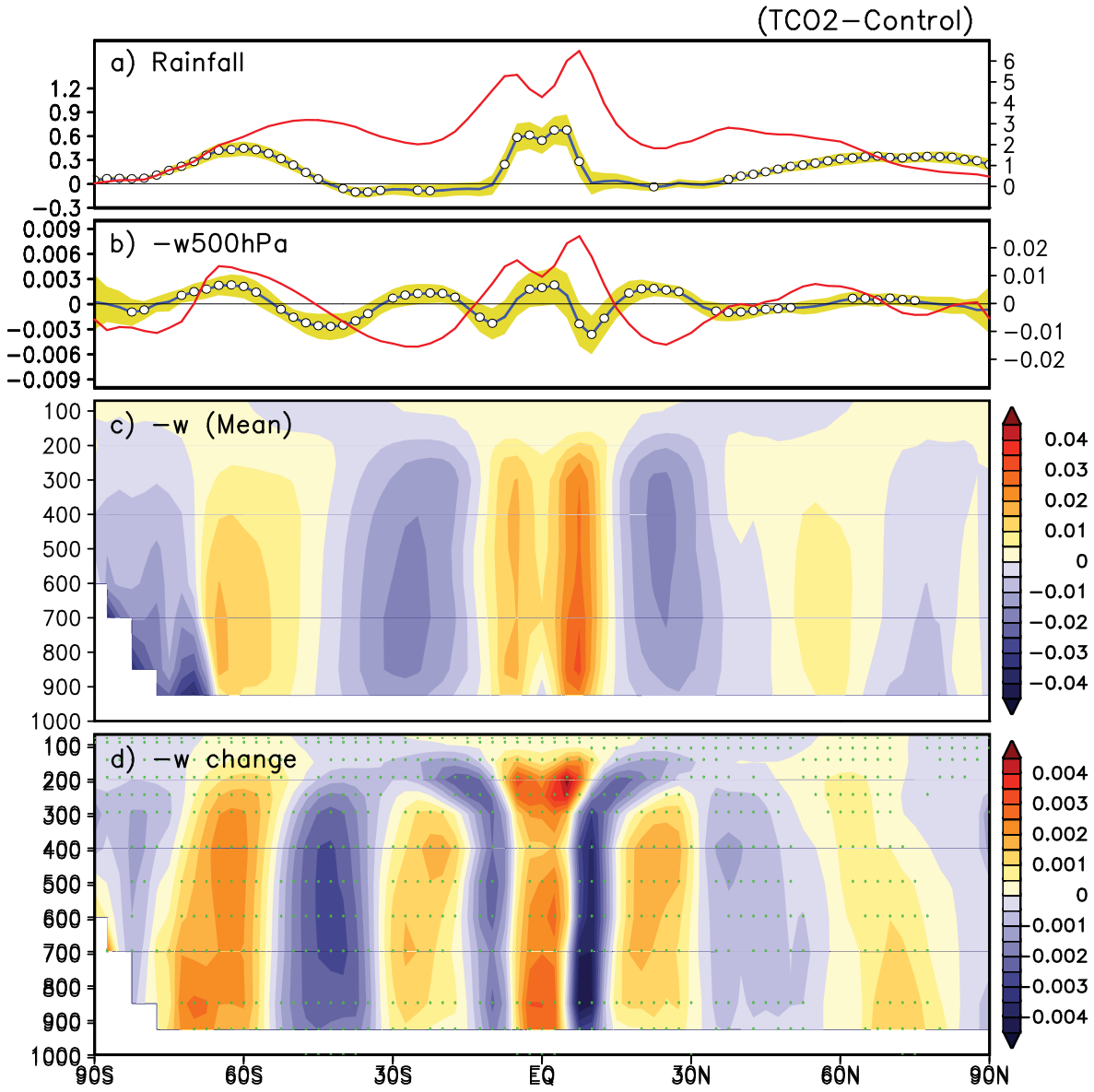

399

400 Figure 2 Latitudinal profile of MMM rainfall (a), and vertical motion (b). Climatology is indicated by
401 red line and anomaly by black line. Open circles indicate where more than 75% (25/33) models
402 agree in the sign of the anomalies. Latitude-height profile of MMM vertical motion for
403 climatology (c) and anomaly (d). Grid points where more than 25 models agree in the sign of the
404 anomaly are indicated by green dots. Rainfall is in unit of mm day^{-1}, and vertical motion is in unit
405 of negative Pa s^{-1}. Different unit scales are used for climatology and anomalies.

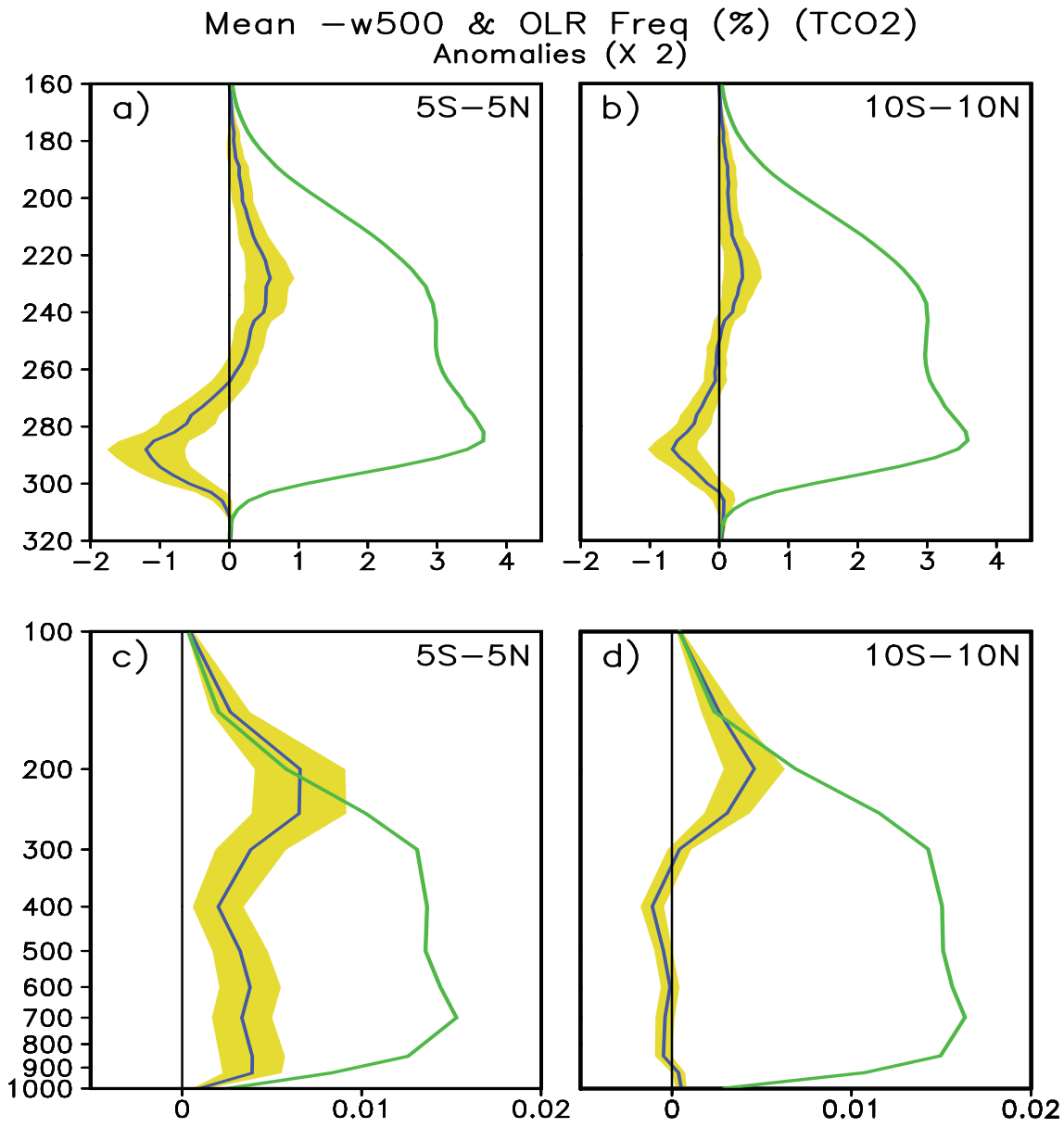

406

407 Figure 3 Vertical profiles of MMM outgoing longwave radiation (OLR) probability distribution
408 function averaged over 5°S-5°N (a), and 10°S-10°N (b). Vertical profile of mean vertical motion
409 averaged over 5°S-5°N (c), and 10°S-10°N (d). Climatology is indicated by green line and anomaly
410 by dotted line. The model spread is shown as yellow shading. The magnitudes of the
411 anomalies have been doubled to enhanced clarity. Vertical motion is in unit of negative Pa s^{-1}.
412 Unit of OLR is Wm^{-2}.

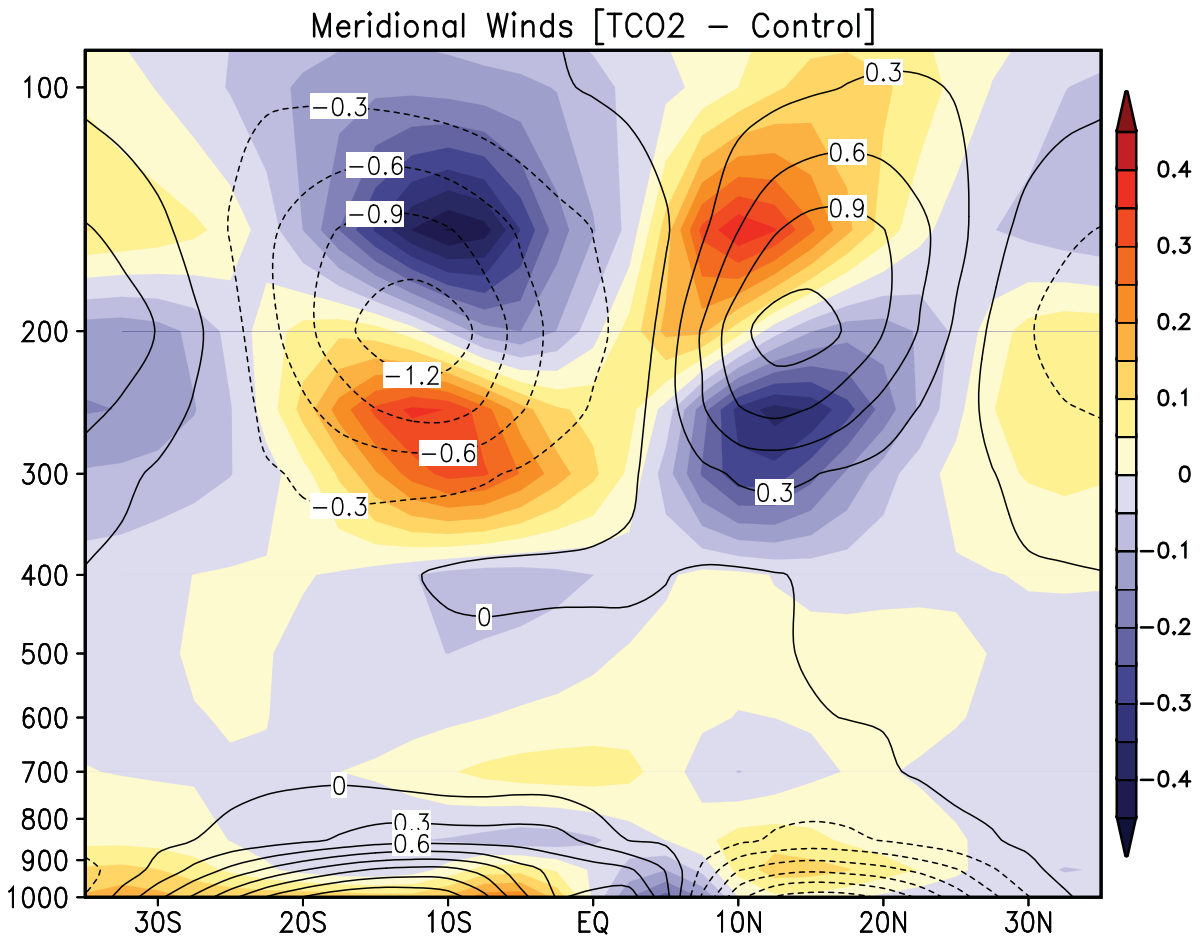

Figure 4 Latitude-height cross-section of MMM meridional winds in the tropics. Climatology is shown in contours, anomaly in color. Unit is in ms^{-1}.

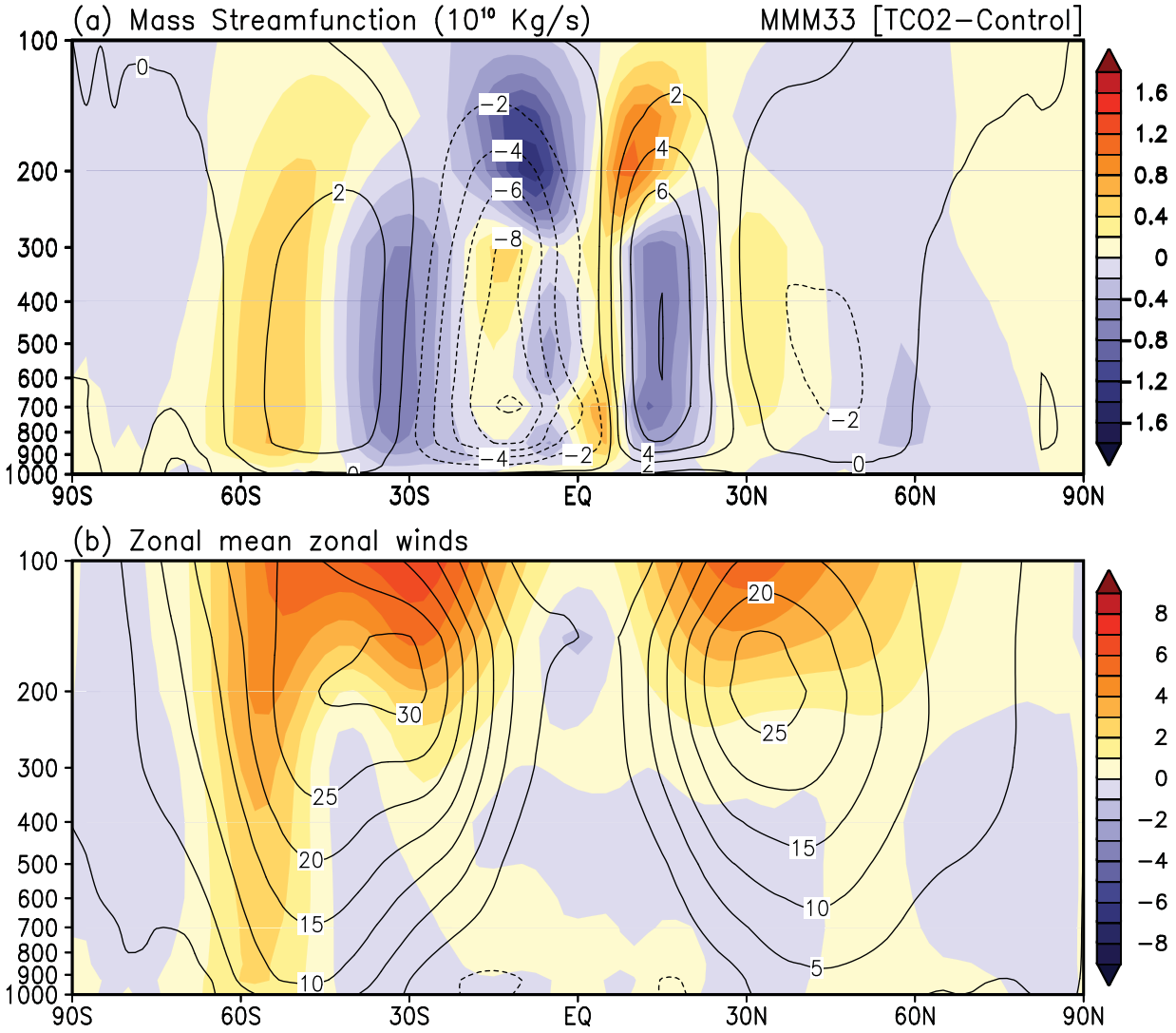

417

418

419 Figure 5 Latitude-height cross-section of MMM for a) merdional mass streamfunction (10^{10} Kg

420 s^{-1}) , and b) zonal mean wind (ms^{-1}). MMM climatology is shown in contour, and anomaly

421 in color. For meridional streamfunction, positive (negative) contours indicate clockwise

422 (anticlockwise) circulation around center of action.

423

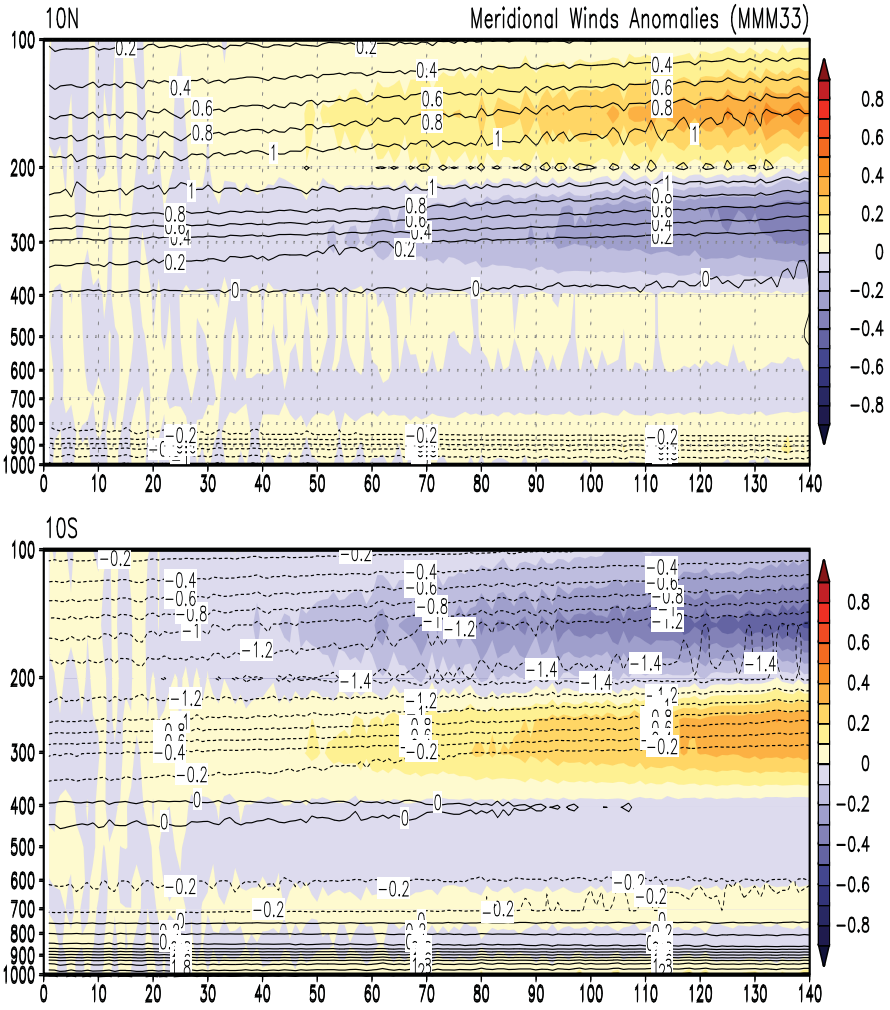

Figure 6 Time-height cross-section of MMM meridional winds (ms^{-1}) for the entire 140 simulated years, under 1% per year CO_2 increase, across a) 10^oN and b) 10^oS. Contours denote the total winds, solid (dotted) lines for positive (negative) winds. Wind anomalies are denoted by color shading. In the northern hemisphere (southern hemisphere), outflow away from the equator is denoted by positive (negative) values, and opposite for inflow toward the equator.